39th AIAA/ASME/SAE/ASEE Joint Propulsion Conference
Huntsville, Alabama, July 20-23, 2003
AIAA-2003-4556

Ion voltage diagnostics in the far-field plume of a high-specific impulse Hall thruster

Richard R. Hofer*
QSS Group, Inc.
NASA Glenn Research Center
Cleveland, OH 44135 USA
richard.hofer@grc.nasa.gov

James M. Haas*
Air Force Research Laboratory
Edwards Air Force Base, CA 93524 USA

Alec D. Gallimore†
Plasmadynamics and Electric Propulsion Laboratory
University of Michigan
Ann Arbor, MI 48109 USA

ABSTRACT

The effects of the magnetic field and discharge voltage on the far-field plume of the NASA-173Mv2 laboratory-model Hall thruster were investigated. A cylindrical Langmuir probe was used to measure the plasma potential and a retarding potential analyzer was employed to measure the ion voltage distribution. The plasma potential was affected by relatively small changes in the external magnetic field, which suggested a means to control the plasma surrounding the thruster. As the discharge voltage increased, the ion voltage distribution showed that the acceleration efficiency increased and the dispersion efficiency decreased. This implied that the ionization zone was growing axially and moving closer to the anode, which could have affected thruster efficiency and lifetime due to higher wall losses. However, wall losses may have been reduced by improved focusing efficiency since the total efficiency increased and the plume divergence decreased with discharge voltage.

I. INTRODUCTION

As used for spacecraft applications in Earth orbit such as station-keeping, orbit-raising, and orbit-transfers, the xenon Hall thruster is most often regarded as a 1600 second specific impulse device operating at discharge voltages of 300 V. Mission studies have shown though that increases in the specific impulse of Hall thrusters to 2000-3000 seconds can enhance or enable a number of Earth-orbital and interplanetary missions.[1-4]

The NASA-173M series of laboratory-model Hall thrusters were conceived in order to understand the design challenges and physical mechanisms determining performance at high-specific impulse (2000-3000 seconds).[5-9] The basic design philosophy was that changes to the magnetic field topography would be required for efficient operation above 1600 seconds specific impulse. Advanced magnetic circuits allowing for *in situ* variation of the magnetic field topography were therefore incorporated into each thruster. The NASA-173Mv1, built jointly by the University of Michigan and the NASA Glenn Research Center (GRC), first established the validity of this approach.[5-6] In a performance study at low current density, changes to the magnetic field topography at high-specific impulse were shown to be critical to achieving efficient operation.[6] The follow-on version, the GRC-developed NASA-173Mv2, incorporated design improvements suggested by its predecessor. A performance mapping of the NASA-173Mv2 at several current densities established that efficient operation at high-specific impulse was possible if a minimum current density was maintained and the magnetic field topography was properly shaped.[7]

Design and experiment have established that Hall thrusters can operate efficiently at high-specific impulse. A need still exists though to improve understanding of the relationship between the thruster design and the microscopic plasma

* Research Engineer, Member AIAA
† Associate Professor, Associate Fellow AIAA

properties. This is necessary to further increase performance, evaluate and improve lifetime, and enable integration with spacecraft. To those ends, a series of plasma diagnostics have been used with the NASA-173Mv2 to better understand the plasma characteristics.[7-9]

In the present work, a retarding potential analyzer was used to measure the ion voltage distribution of the NASA-173Mv2 Hall thruster. A cylindrical Langmuir probe was also used to obtain the plasma potential so that the true ion voltage distribution could be calculated. The ion voltage distribution is of interest because it is used by spacecraft designers to calculate plume impingement on sensitive surfaces (e.g., solar arrays and optics), as well as by thruster designers to quantify how changes to the operating point or thruster hardware affect lifetime and performance. The goal of these experiments was to gain insight on how the plasma potential in the thruster plume and the ionization and acceleration processes internal to the thruster were affected by changes of the magnetic field and discharge voltage.

II. EXPERIMENTAL APPARATUS

The thruster hardware and configuration were the same as the experiments reported in Ref. 7. This included the thruster, power electronics, vacuum facility, and the thruster mounting scheme in the vacuum facility. In the experiments reported here, a Langmuir probe and retarding potential analyzer were added two meters downstream of the thruster.

A. NASA-173Mv2 Hall effect thruster

The laboratory model NASA-173Mv2 is a 5 kW-class Hall thruster that has a discharge chamber outer diameter of 173 mm (Figure 1; see Ref. 7 for a detailed description). A fixed structure of magnetic poles pieces, an inner coil (IC) and an outer coil (OC) are used to form the primary magnetic circuit. Fine control of the magnetic field is provided with an internal trim coil (ITC) and an external trim coil (ETC). The ITC primarily affects the radial magnetic field in the discharge chamber, while the ETC affects the magnetic field downstream of the exit plane and near the cathode.

Figure 2 shows the total specific impulse and total efficiency of the NASA-173Mv2 at 10 mg/s versus discharge voltage.[7] The specific impulse and efficiency include the cathode flow and the efficiency also includes the power to the magnets. Specific impulse and efficiency range from 1600-3400 seconds and 51-61%, respectively, over voltages of 300-1000 V. The use of trim coils increases efficiency by 1-2%. The trim coils also decrease plume divergence and the frequency and magnitude of plasma oscillations.[7]

Figure 1 - Photograph of the NASA-173Mv2 Hall thruster.

The plasma discharge was powered by a matching pair of commercially available power supplies wired in series that provided a 1200 V, 16 A output. The discharge filter consisted of a 100 μF capacitor in parallel with the supply outputs. Other commercially available power supplies were used to power the magnet coils and the cathode heater and keeper. The laboratory-model hollow cathode was a GRC design capable of emission currents up to 20 A. As shown in Figure 1, the cathode was positioned above the thruster.

High-purity xenon was supplied through stainless steel feed lines with 20 and 200 sccm mass flow controllers. The controllers were calibrated before the experiments using a constant-volume method. Based on the calibrations, the uncertainty was estimated as ±0.7% for the anode flow rate and ±1.4% for the cathode flow rate.

Thruster telemetry was acquired using a 22-bit datalogger. The DC accuracy of the unit, as reported by the manufacturer, is 0.004%. However, calibration of each channel using digital multimeters increased the uncertainty to ±0.05% for voltage and ±0.2% for current.

The thruster was operated for four hours after initial exposure to vacuum conditions to allow for outgassing of the chamber walls. Upon subsequent thruster shutdowns and restarts or a change in the discharge voltage, the thruster was operated for at least 30-60 minutes before data was acquired. This procedure allowed enough time for the discharge current to reach a steady-state value.

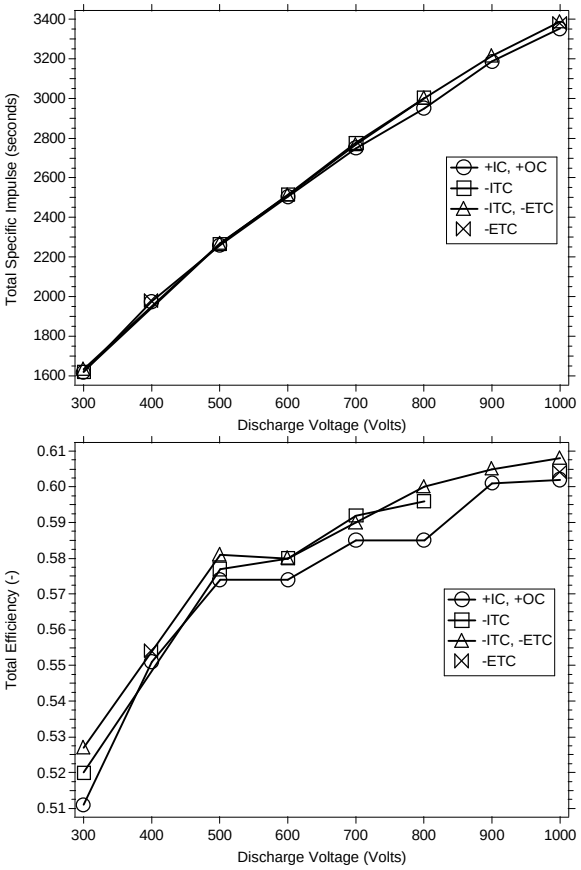

Figure 2 - Total specific impulse and efficiency versus discharge voltage of the NASA-173Mv2 at 10 mg/s. (from Ref. 7)

B. Vacuum facility

All experiments were conducted in vacuum facility 12 (VF12) at GRC. VF12 is a cylindrical, stainless steel chamber 3.0 m in diameter by 9.6 m in length. The facility is cryogenically pumped and backed by a turbomolecular pump for removal of gases not pumped by the cryosurfaces. The thruster was mounted on the thrust stand described in Ref. 7. The thrust stand pendulum was locked down and not used for these experiments. In this position, the thruster was near the chamber's vertical centerline and fired 8.9 m down the length of the tank toward the pumps, which are located along the back half of the chamber. A hot-cathode ionization gauge was mounted 0.4 m below the vertical chamber centerline, 5.2 m downstream of the thruster. Pressure measurements were corrected for xenon using the base pressure on air and a correction factor of 2.87 for xenon. For a total xenon flow rate of 11 mg/s, the pressure was 4.6×10^{-6} Torr, after correcting for xenon and the base pressure on air, which was 1.0×10^{-7} Torr. This corresponded to a xenon pumping speed of 340,000 l/s.

C. Cylindrical Langmuir probe

A cylindrical Langmuir probe was used to measure the plasma potential (V_p) with respect to facility ground near the location of the RPA. As described in the next section, the plasma potential was needed to obtain the true ion voltage. The measurements were taken during experiments with an ExB probe, which are described in Ref. 9.

The Langmuir probe had a diameter of 1.60 mm and a length of 16.5 mm. The length of the probe was aligned parallel to the ion flow, with the mid-point located 2 m downstream of the thruster exit plane and 6 cm radially from thruster centerline. This probe placement meant that the Langmuir probe sampled the plasma at a different radial location than the RPA. Data from the P5 Hall thruster, which also has an outer diameter of 173 mm, has shown that the plasma potential varies only by a few volts over large angular positions from centerline.[10] Based on the P5 data, the uncertainty due to the Langmuir probe not having been in the same position as the RPA was estimated to be less than one volt.

The magnetic field leaking from the permanent magnets in the ExB probe was on the order of a few Gauss. This was sufficiently small that magnetic field effects could be neglected in the analysis of the probe characteristic.

The plasma potential was found from the maximum in the first derivative of the electron

current. This method was easily automated in the data analysis, but tended to underestimate the plasma potential when compared to graphical analysis using curve fitting.[11] Comparisons between the different methods on a few test cases showed that the derivative method was consistently lower than the graphical method by a value on the order of a volt.

Considering all the error sources described above, the uncertainty in the plasma potential was estimated to be +2/-1 V.

D. Retarding potential analyzer

1. Theory

A retarding potential analyzer (RPA) selectively filters ions by applying a retarding potential across an inlet grid.[12-15] The probe acts as a high-pass filter by allowing only ions with voltages (i.e., energy to charge ratios, V=E/q) greater than the grid voltage to pass and reach a collection electrode. The derivative of the resulting current-voltage characteristic (dI/dV) is proportional to the ion voltage distribution function (f(V)) given by,

$$\frac{dI}{dV} = -\frac{q_i^2 e^2 n_i A_c}{m_i} f(V) \qquad (1)$$

where q_i is the charge-state of the ion, e is the elementary charge, n_i is the ion density, A_c is the probe collection area, and m_i is the ion mass.[12] A RPA measures the ion energy distribution only if the plasma is composed of ions of the same mass and charge. This is not the case for xenon Hall thrusters, which for 300 V discharges are composed of 4-11% Xe^{2+} and 1% Xe^{3+}.[9-10,12] Further, the Xe^{2+} fraction of the NASA-173Mv2 has recently been measured to vary from 4% at 300 V to 12 % at 900 V.[9] When used with Hall thrusters, a RPA therefore measures the ion voltage distribution function unless a time-of-flight method, such as the one described in Ref. 13, is used to discriminate the individual charge-state of the ions.

2. Design

The RPA used in these experiments was provided by the Air Force Research Laboratory. Shown schematically in Figure 3, the three-grid RPA design was based on the multi-gridded energy analyzer in Ref. 14. The outer body of the RPA was constructed of 316 stainless steel tubing and was grounded to the vacuum facility. A phenolic sleeve placed inside the body provided electrical isolation of the grids. All grids were made from 316 stainless steel, photochemically machined sheet with a thickness of 0.1 mm. The grid openings were 0.3 mm diameter with a total open area fraction of 38%. Grid spacing was achieved using glass-mica ceramic washers and the ion collector was a copper disk. Electrical connections were accomplished by spot welding stainless steel wire to each grid. The wires were then routed along the inner edge of the phenolic sleeve and out the rear of the body. The washers and grids were fixed in place by a spring placed between the collector and a rear cover. Relevant dimensions are summarized in Table 1.

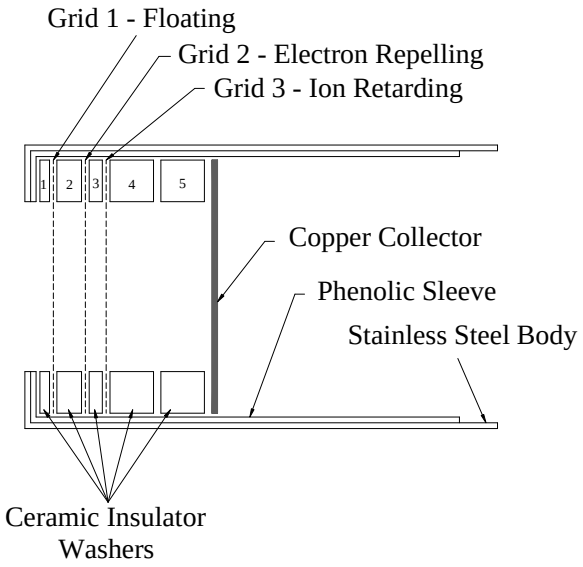

Figure 3 - Schematic of the RPA.

Table 1 - RPA washer dimensions.

Washer	Thickness (mm)	Inner Diameter (mm)
1	1.0	18.6
2	3.4	21.6
3	1.7	21.7
4	6.5	21.4
5	6.5	21.5

During operation, grid 1 was electrically isolated from the probe and facility ground to

minimize perturbation between the probe and ambient plasma. Grid 2 was biased -30 V below ground to repel incident electrons. An electric potential ranging from 0-1100 V relative to ground was applied to grid 3 using a high-voltage power supply. The ion current to the collector was measured using a picoammeter. Figure 4 shows the RPA electrical schematic.

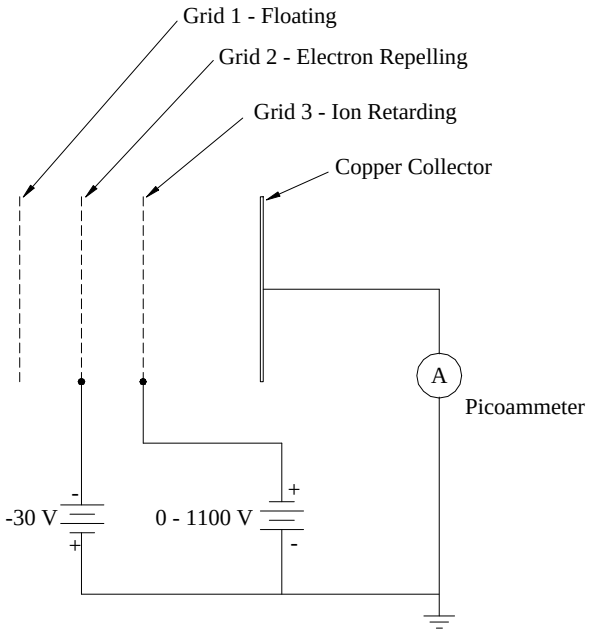

Figure 4 - RPA electrical schematic.

3. Data interpretation

The RPA measured the ion voltage with respect to facility ground. As shown in the potential diagram of Figure 5, the true ion voltage (V_{true}) was obtained by subtracting the plasma potential from the measured value (V_{rpa}).

$$V_{true} = V_{rpa} - V_p \qquad (2)$$

To characterize the acceleration efficiency given by,[16]

$$h_a = \frac{\langle e_i \rangle}{eV_d} \qquad (3)$$

(where $\langle \varepsilon_i \rangle$ is the mean ion energy and V_d is the discharge voltage) the most-probable ion voltage (V_{mp}) and the loss voltage (V_{loss}) were found from the ion voltage distribution. The most-probable ion voltage was defined as the voltage where the ion current was greatest. The loss voltage was then computed as the difference between the discharge voltage (V_d) and the most-probable voltage.

$$V_{loss} = V_d - V_{mp} \qquad (4)$$

The most-probable ion voltage and the loss voltage can be used to approximate the acceleration efficiency because,

$$h_a \approx \frac{V_{mp}}{V_d} = 1 - \frac{V_{loss}}{V_d} \qquad (5)$$

Equation 5 is an approximation because the mean ion energy and the most-probable voltage will differ by a few volts due to the effects of multiply-charged ions and collisions.

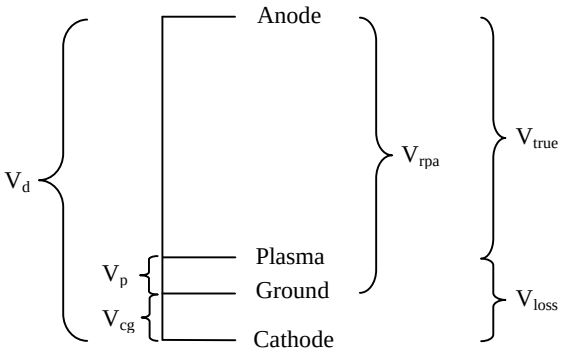

Figure 5 - Potential diagram showing the relationship between the measured quantities (V_{rpa}, V_p, V_{cg}, V_d), the true ion voltage (V_{true}), and the loss voltage (V_{loss}).

The spread in ion velocities (or energy) is given by the dispersion efficiency,

$$h_d = \frac{\langle U_i \rangle^2}{\langle U_i^2 \rangle} \qquad (6)$$

(where U_i is the ion velocity).[16] The dispersion efficiency was characterized by the full width at half-maximum (FWHM) of the ion voltage distribution,

$$FWHM = V\big|_{(I_{max}/2)^+} - V\big|_{(I_{max}/2)^-} \qquad (7)$$

i.e., the FWHM was defined as the difference in volts above (+) and below (-) the most-probable voltage where the ion current fell to one-half its maximum value (I_{max}). Measurement uncertainty from probe-induced signal broadening (see section II.D.4) did not allow the ion voltage distributions

to be used in calculating the dispersion efficiency. However, the FWHM was still useful in observing the relative variation of the dispersion efficiency with operating point.

4. Measurement Uncertainty

The RPA was compared to a 45º parallel-plate electrostatic energy analyzer (ESA) in Ref. 15. In those experiments, both instruments collected plume data 0.5 m downstream of a Busek BHT-200-X3 Hall thruster operated at a discharge voltage of 250 V. Figure 6 shows the distributions measured with respect to facility ground by the RPA and the ESA on thruster centerline. A comparison of the most-probable voltage and FWHM from the different instruments are used here to assess their relative accuracy.

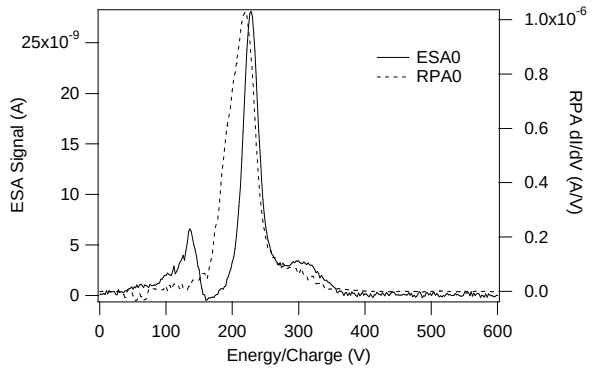

Figure 6 - Ion voltage distributions measured with the RPA and a parallel-plate energy analyzer on the centerline of the Busek BHT-200-X3 Hall thruster, 0.5 m downstream of the exit plane. (from Ref. 15)

As Figure 6 shows, the most-probable ion voltage measured by the two instruments was in good agreement. The RPA measured a most-probable voltage of 220 V and the ESA was 3.6% higher, or 228 V. In contrast, the FWHM from the two instruments showed significant differences. The FWHM measured by the RPA was 45 V and the ESA was 42% lower, or 26 V. The differences can be attributed to instrument broadening in the RPA and, to a lesser extent, the effects of numerical differentiation and spline curve-fitting (see section III.B). Instrument broadening in the RPA could have been due to pressure build-up inside the probe and/or the large acceptance half-angle of the probe (45º in the RPA versus 4º in the ESA). Regardless of the exact cause, the FWHM of the RPA was considered an upper-bound of the true FWHM. Considering the results in Ref. 15 and the experiments reported here, the uncertainties of the most-probable voltage and the FWHM was estimated as ±10 V and +0/-20 V, respectively.

III. RESULTS

Langmuir probe and RPA measurements were taken during separate testing periods with the thruster operating at an anode flow rate of 10.0 mg/s and a cathode flow rate of 1.0 mg/s. Langmuir probe measurements were taken for discharge voltages of 300-1000 V, while the RPA measurements spanned 300-800 V. A grid short with the RPA ended testing at 800 V. The axial placement of both probes was 2 m downstream of the thruster exit plane. In the radial direction, the RPA was positioned on the thruster centerline while the Langmuir probe was placed 6 cm from centerline. At each discharge voltage, the effects of the magnetic field were evaluated by using several combinations of the thruster coils. The coil combinations were:

1. with the IC and OC only (+IC, +OC),
2. with the IC, OC, and ITC (-ITC),
3. with the IC, OC, ITC, and ETC (-ITC, -ETC), and
4. with the IC, OC, and ETC (-ETC).

With the exception of the -ETC points, the coil currents were taken from a performance characterization that showed these settings maximized thruster efficiency.[7] The symbols "+" or "-" indicate the polarity of a coil, where "+" adds and "-" subtracts from the magnetic field. Thruster telemetry for both test series are in the appendix as Table 2. Results from the probe measurements are in the appendix as Table 3.

A. Plasma potential

Figure 7 plots the plasma potential with respect to facility ground versus the discharge voltage and magnetic field. Regardless of the magnetic field, the plasma potential increased 3-4 V as the discharge voltage increased from 300-1000 V. At a given discharge voltage, changing the magnetic field with the ETC decreased the plasma potential by 1-2 V while the ITC had no apparent effect.

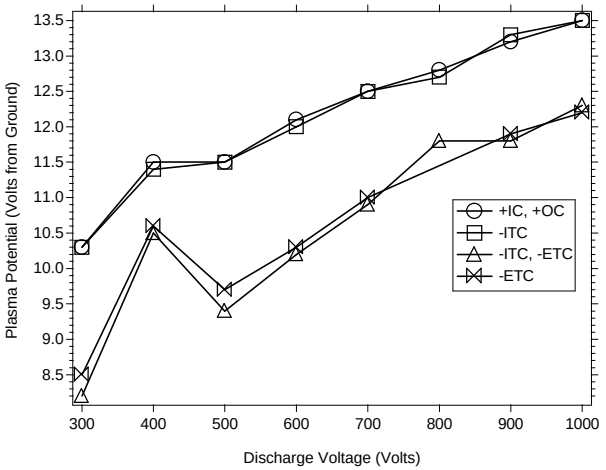

Figure 7 - Plasma potential versus discharge voltage and magnetic field, two meters from the thruster. Changing the magnetic field with the external trim coil (ETC) decreased the plasma potential by 1-2 volts.

B. Ion voltage distribution

At each discharge voltage and magnetic field, three sweeps of the ion retarding voltage were performed with the RPA. The resulting I-V curves were found to be very repeatable. Figure 8 shows the raw data from voltage sweeps when the inner and outer coils were energized (+IC, +OC). Except for 800 V (where a grid short occurred after one sweep), each curve in Figure 8 consists of the data from three separate sweeps.

For a given voltage and magnetic field, each sweep of the RPA was averaged together, curve-fit using a smoothing spline algorithm,[17] and then numerically differentiated. The spline was used to reduce noise caused by the differentiation. Lastly, the plasma potential was subtracted from the retarding voltage to yield the true ion voltage distribution. In Figure 9, the effects of the spline are compared to the raw data for discharge voltages of 300 and 700 V (+IC, +OC). The spline operation induced enough smoothing that detailed features (e.g., charge-exchange collision signatures) were not resolved. However, the most-probable ion voltage and the FWHM were relatively insensitive to the smoothing parameters. The uncertainty in the most-probable ion voltage and the FWHM from the spline operation was estimated as ±0.5% and ±1% of the discharge voltage, respectively. The uncertainty estimates were based on numerical experiments that examined how the two quantities depended on the smoothing parameters. The uncertainty from the spline operation was included in the overall uncertainty estimates discussed in section II.D.4.

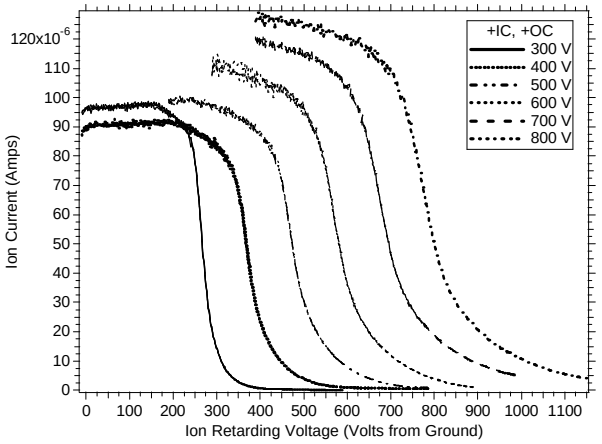

Figure 8 - Ion current versus retarding voltage from the RPA (+IC, +OC) for discharge voltages of 300-800 V. To demonstrate repeatability, data from multiple sweeps are overlaid at each discharge voltage, except 800 V where only one sweep was obtained.

Figure 10 shows the ion voltage distribution (normalized to the peak ion current) at each thruster operating point. The coil configurations are not delineated in the figure because the differences were indistinguishable at the chosen scale.

From each of the distributions in Figure 10, the most-probable voltage, the loss voltage and the FWHM were calculated. Figure 11 shows the loss voltage and Figure 12 shows the FWHM versus discharge voltage and magnetic field. There was no systematic dependence of the loss voltage with the magnetic field. The loss voltage decreased with discharge voltage from 35 V at 300 V to 25 V at 800 V, which translated into an increase in the acceleration efficiency from 88±3% at 300 V, to 97±1% at 800 V. The FWHM increased with discharge voltage by over a factor of three from 33 V at 300 V to 105 V at 800 V. The increase in the FWHM correlated with measurements using an ExB probe that showed the same trend.[9] Changes in the magnetic field due to the ETC decreased the FWHM by 3-4 V on average.

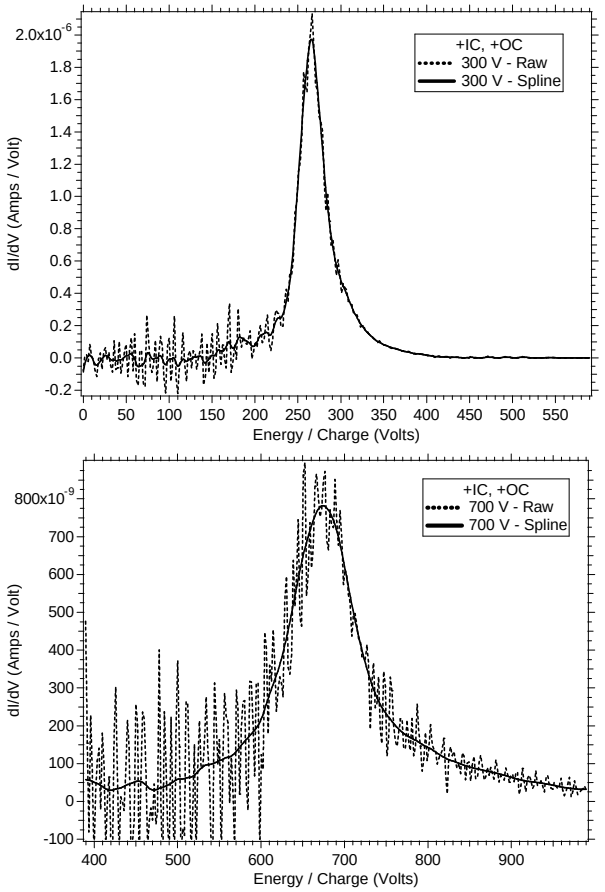

Figure 9 – Representative ion voltage distributions showing the raw data and the spline fit to the data for discharge voltages of 300 and 700 V (+IC, +OC).

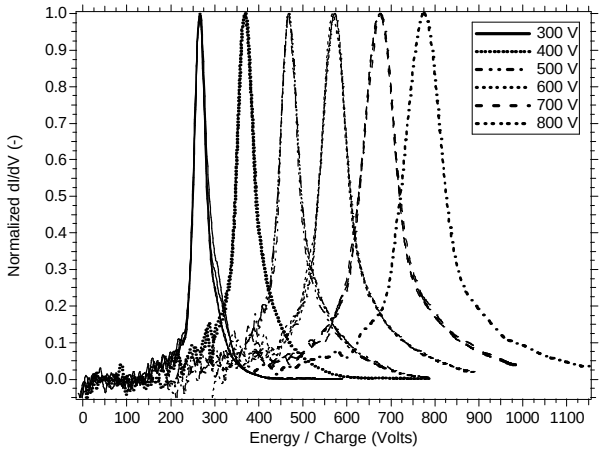

Figure 10 - Normalized ion voltage distributions versus discharge voltage.

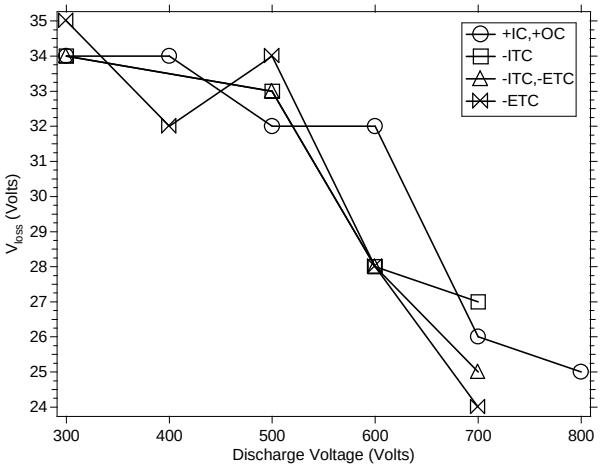

Figure 11 - Loss voltage versus discharge voltage and magnetic field.

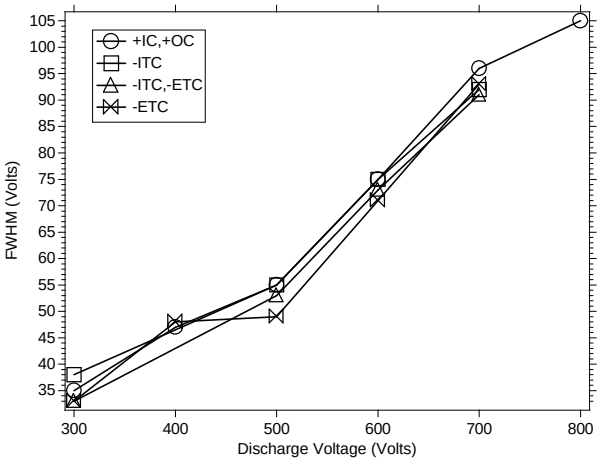

Figure 12 - The full-width at half-maximum (FWHM) of the ion voltage distributions versus discharge voltage and magnetic field.

IV. DISCUSSION

A. Plasma potential

Figure 7 shows that the plasma potential ranged from 8.2-13.5 V as the discharge voltage increased from 300-1000 V. While still small compared to the discharge voltage, the plasma potential was a significant fraction of the loss voltage. These findings highlight the importance of knowing the true ion voltage to reduce uncertainty in the loss voltage; i.e., the acceleration efficiency.

A remarkable feature of Figure 7 is the 1-2 V decrease in plasma potential caused by changing

the magnetic field with the ETC.[#] The decrease in plasma potential might at first seem unlikely because of the relatively large distance involved (~12 thruster diameters) and the small change in the magnetic field caused by the ETC (5-10% of the peak field at the exit plane). However, the trends are consistent with the numerical modeling in Ref. 18, which showed that a decreasing magnetic field would decrease the plasma potential in the thruster plume, albeit at smaller rates (about 0.03 V/G compared to 0.1-0.2 V/G from the results presented here). The ability to influence the plasma potential with external magnetics could be used to control the plasma near the thruster. This has important implications regarding spacecraft integration and thruster lifetime. Additional experiments are planned to investigate magnetic field effects on the plasma potential distribution in the thruster plume.

B. Ion voltage distribution

1. Effects of the magnetic field

Changes in the magnetic field resulted in marginal changes to the ion voltage distribution. Of all the coil combinations that were used, only the ETC consistently changed the distributions by decreasing the FWHM. It may be that the dependence of the ion voltage distribution on the magnetic field was obscured by measurement uncertainty. Experiments with an electrostatic energy analyzer are planned that should better resolve the effects of the magnetic field.

2. Effects of the discharge voltage

The acceleration and dispersion efficiencies (η_a and η_d) are primarily affected by changes to the centroid position (Z_i and Z_a) or the length (L_i and L_a) of the ionization and acceleration zones. In Hall thrusters, the two zones overlap such that η_a and η_d are always less than unity. If L_a and Z_a are unchanged, efficiency improvements are possible if L_i decreases and Z_i is positioned further upstream of the acceleration zone. However, due to the competing effects of wall losses, the maximum total thruster efficiency does not correspond to the complete separation of the two zones. This is because moving the ionization zone away from the acceleration zone can increase the rate at which ions are lost to the walls. Thus, the optimum configuration in a Hall thruster would seem to be highly peaked ionization and acceleration zones with the ionization zone located as close to the beginning of the acceleration zone as possible.

As the discharge voltage increased in these experiments, η_a increased and η_d decreased. There are several ways that Z_i, Z_a, L_i, and L_a can change to produce these results. Before considering these, it is helpful to review the results from Ref. 8, which presented measurements of the discharge chamber floating potential and visual observations of the plasma in the discharge chamber. Results from Ref. 8 indicated that as the discharge voltage increased:

1) L_a was approximately constant,
2) Z_a moved upstream by 3±1 mm, and
3) either Z_i moved upstream or L_i increased in length towards the anode. This was inferred from visual observations of the plasma, so it was not possible to determine if the movement resulted from a shift in Z_i or growth of L_i. (Note that an increase of L_i in only one direction must also shift Z_i.)

The results from Ref. 8 are useful in determining the source of changes in η_a and η_d. In general, an increase in η_a may result if:

a) Z_i moves upstream,
b) L_i grows in the direction of the anode,
c) Z_a moves downstream, or
d) L_a decreases.

From Ref. 8, 1) and 2) eliminate d) and c), respectively, while 3) supports either a) or b). Therefore, the increase in the acceleration efficiency can be attributed to either a shift or lengthening of the ionization zone towards the anode.

In general, a decrease in η_d may result if:

i) Z_i moves downstream,
ii) L_i increases,
iii) Z_a moves upstream, or
iv) L_a increases.

From Ref. 8, 1) eliminates iv), 3) eliminates i) and supports ii), and 2) supports iii).

[#] At 400 V, the decrease in plasma potential was smaller than the other discharge voltages most likely because the ETC current was less (-2 A at 400 V versus -4 to -6 A at all other voltages).

Therefore, the decrease in the dispersion efficiency can be attributed either to the movement of the acceleration zone or growth of the ionization zone. However, because a shift in the position of the acceleration zone towards the anode would also decrease the acceleration efficiency (the opposite was observed), it was more likely that changes to the position and length of the ionization zone were the primary factors driving the observed changes in the acceleration and dispersion efficiencies.

In general, a longer ionization zone could be detrimental to thruster efficiency and lifetime due to higher wall losses. However, because the total efficiency increased with discharge voltage, additional wall losses may have been reduced by better focusing efficiency. This would be consistent with the decrease of plume divergence from 38º to 28º at voltages of 400-1000 V measured in Ref. 7.

ACKNOWLEDGEMENTS

Program support for this research through Code R Energetics funding is gratefully acknowledged.

REFERENCES

1. Noca, M., Brophy, J. R., "Over Powering Solar System Exploration," AIAA-1997-2914, 33rd Joint Propulsion Conference, Seattle, WA, July 6-9, 1997.
2. Oleson, S. R., "Advanced Electric Propulsion for Space Solar Power Satellites," AIAA-1999-2872, 35th Joint Propulsion Conference, Los Angeles, CA, June 20-24, 1999.
3. Oleson, S. R., "Mission Advantages of Constant Power, Variable Isp Electrostatic Thrusters," AIAA-2000-3413, 36th Joint Propulsion Conference, Huntsville, AL, July 17-19, 2000.
4. Fiehler, D. I., Oleson, S. R., "A Comparison of Electric Propulsion Systems for Mars Exploration," AIAA-2003-4574, 39th Joint Propulsion Conference, Huntsville, AL July 20-23, 2003.
5. Hofer, R. R., Peterson, P. Y., Gallimore, A. D., "A High Specific Impulse Two-Stage Hall Thruster with Plasma Lens Focusing," IEPC-01-036, 27th International Electric Propulsion Conference, Pasadena, CA, Oct 14-19, 2001.
6. Hofer, R. R., Gallimore, A. D., "The Role of Magnetic Field Topography in Improving the Performance of High-Voltage Hall Thrusters," AIAA-2002-4111, 38th Joint Propulsion Conference, Indianapolis, IN, July 7-10, 2002.
7. Hofer, R. R., Jankovsky, R. S., "The Influence of Current Density and Magnetic Field Topography in Optimizing the Performance, Divergence, and Plasma Oscillations of High Specific Impulse Hall Thrusters," IEPC-03-142, 28th International Electric Propulsion Conference, Toulouse, France, March 17-21, 2003.
8. Hofer, R. R., Gallimore, A. D., "Recent Results from Internal and Very-Near-Field Plasma Diagnostics of a High Specific Impulse Hall Thruster," IEPC-03-037, 28th International Electric Propulsion Conference, Toulouse, France, March 17-21, 2003.
9. Hofer, R. R., Gallimore, A. D., "Ion species fractions in the far-field plume of a high-specific impulse Hall thruster," AIAA-2003-5001, 39th Joint Propulsion Conference, Huntsville, AL July 20-23, 2003.
10. Gulczinski, F.S., "Examination of the Structure and Evolution of Ion Energy Properties of a 5 kW Class Laboratory Hall Effect Thruster at Various Operational Conditions," Ph.D. Dissertation, University of Michigan, 1999.
11. Lochte-Holtgreven, W., ed., Plasma Diagnostics, American Elsevier Publishing, New York, 1968.
12. King, L.B., "Transport-property and Mass Spectral Measurements in the Plasma Exhaust Plume of a Hall-effect Space Propulsion System," Ph.D. Dissertation, University of Michigan, 1998.
13. Prioul, M., et al., "Insights on Physics of Hall Thrusters through Fast Current Interruptions and Discharge Transients," IEPC-01-059, 27th International Electric Propulsion Conference, Pasadena, CA, Oct 14-19, 2001.
14. Hutchinson, I. H., Principles of Plasma Diagnostics, Cambridge University Press, New York, 2002.
15. Beal, B. E., Gallimore, A. D., "Energy Analysis of a Hall Thruster Cluster," IEPC-03-35, 28th International Electric Propulsion Conference, Toulouse, France, March 17-21, 2003.
16. Kim, V., "Main Physical Features and Processes Determining the Performance of Stationary Plasma Thrusters," Journal of Propulsion and Power, Vol. 14, No. 5, Sept-Oct, 1998, pp. 736-743.
17. Reinsch, Christian H., "Smoothing by Spline Functions," Numerische Mathematic 10, pp. 177-183, 1967.
18. Keidar, M., Boyd, I. D., "Effect of a Magnetic Field on the Plasma Plume from Hall Thrusters," Journal of Applied Physics, Vol. 86, No. 9, November 1, 1999.

APPENDIX

Table 2 - NASA-173Mv2 telemetry from Langmuir probe and RPA measurements.

Thruster Telemetry from Langmuir Probe Measurements

Point	Vd (V)	Id (A)	Anode (mg/s)	Cathode (mg/s)	Inner Coil (A)	Outer Coil (A)	Internal Trim Coil (A)	External Trim Coil (A)	Vcg (V)	Pressure (Torr)
148	300.3	9.00	10.00	1.00	1.75	1.50	0.00	0.00	-11.3	4.6E-06
149	300.4	8.89	10.00	1.00	1.75	1.50	-0.54	0.00	-11.2	4.6E-06
150	300.4	8.88	10.00	1.00	1.75	1.50	-0.54	-4.00	-10.6	4.6E-06
151	300.4	8.99	10.00	1.00	1.75	1.50	0.00	-4.00	-10.9	4.6E-06
152	400.2	9.32	10.00	1.00	2.50	2.26	0.00	0.00	-12.7	4.6E-06
153	400.2	9.26	10.00	1.00	2.50	2.26	-0.36	0.00	-12.7	4.6E-06
154	400.2	9.25	10.00	1.00	2.50	2.26	-0.36	-2.00	-12.3	4.6E-06
155	400.2	9.32	10.00	1.00	2.50	2.26	0.00	-2.00	-12.2	4.6E-06
156	500.3	9.49	10.00	1.00	3.00	2.20	0.00	0.00	-13.2	4.6E-06
157	500.3	9.34	10.00	1.00	3.00	2.20	-0.35	0.00	-13.4	4.6E-06
158	500.3	9.42	10.00	1.00	3.00	2.20	-0.35	-5.00	-12.7	4.6E-06
159	500.3	9.46	10.00	1.00	3.00	2.20	0.00	-5.00	-12.6	4.6E-06
160	600.3	9.41	10.00	1.00	3.26	2.49	0.00	0.00	-13.0	4.6E-06
161	600.3	9.24	10.00	1.00	3.26	2.49	-0.26	0.00	-13.5	4.6E-06
162	600.3	9.35	10.00	1.00	3.26	2.49	-0.26	-5.00	-12.9	4.6E-06
163	600.3	9.46	10.00	1.00	3.26	2.49	0.00	-5.00	-12.4	4.6E-06
164	700.3	9.40	10.00	1.00	3.41	3.06	0.00	0.00	-14.3	4.6E-06
165	700.3	9.53	10.00	1.00	3.41	3.06	-0.20	0.00	-14.1	4.6E-06
166	700.3	9.51	10.00	1.00	3.41	3.06	-0.20	-5.00	-13.8	4.6E-06
168	700.5	9.54	10.00	1.00	3.41	3.06	0.00	-5.00	-13.3	4.6E-06
170	800.1	9.44	10.00	1.00	3.82	3.30	0.00	0.00	-14.7	4.6E-06
171	800.1	9.55	10.00	1.00	3.82	3.30	-0.21	0.00	-14.5	4.6E-06
172	800.1	9.53	10.00	1.00	3.82	3.30	-0.21	-5.00	-13.9	4.6E-06
175	900.4	9.61	10.00	1.00	3.85	3.61	0.00	0.00	-13.8	4.6E-06
176	900.4	9.72	10.00	1.00	3.85	3.61	-0.04	0.00	-13.8	4.6E-06
177	900.4	9.73	10.00	1.00	3.85	3.61	-0.04	-5.90	-13.3	4.6E-06
178	900.4	9.73	10.00	1.00	3.85	3.61	0.00	-5.90	-13.3	4.6E-06
181	1000.1	9.71	10.00	1.00	4.36	3.81	0.00	0.00	-14.2	4.6E-06
182	1000.1	9.85	10.00	1.00	4.36	3.81	-0.16	0.00	-13.8	4.6E-06
183	1000.1	9.94	10.00	1.00	4.36	3.81	-0.16	-5.00	-13.1	4.6E-06
184	1000.1	10.08	10.00	1.00	4.36	3.81	0.00	-5.00	-12.9	4.6E-06

Thruster Telemetry from RPA Measurements

Point	Vd (V)	Id (A)	Anode (mg/s)	Cathode (mg/s)	Inner Coil (A)	Outer Coil (A)	Internal Trim Coil (A)	External Trim Coil (A)	Vcg (V)	Pressure (Torr)
70	300.2	8.86	10.00	1.00	1.75	1.50	0.00	0.00	-11.9	4.6E-06
71	300.2	8.68	10.00	1.00	1.75	1.50	-0.54	0.00	-11.9	4.6E-06
72	300.1	8.68	10.00	1.00	1.75	1.50	-0.54	-4.00	-11.5	4.6E-06
73	300.2	8.88	10.00	1.00	1.75	1.50	0.00	-4.00	-11.5	4.6E-06
74	400.4	9.24	10.00	1.00	2.50	2.26	0.00	0.00	-12.7	4.6E-06
75	400.4	9.24	10.00	1.00	2.50	2.26	0.00	-2.00	-12.7	4.6E-06
76	500.4	9.38	10.00	1.00	3.00	2.20	0.00	0.00	-13.2	4.6E-06
77	500.3	9.23	10.00	1.00	3.00	2.20	-0.35	0.00	-13.1	4.6E-06
78	500.4	9.29	10.00	1.00	3.00	2.20	-0.35	-5.00	-13.1	4.6E-06
79	500.4	9.43	10.00	1.00	3.00	2.20	0.00	-5.00	-13.3	4.6E-06
82	600.3	9.53	10.00	1.00	3.26	2.49	0.00	0.00	-13.1	4.6E-06
83	600.3	9.47	10.00	1.00	3.26	2.49	-0.26	0.00	-12.8	4.6E-06
84	600.3	9.51	10.00	1.00	3.26	2.49	-0.26	-5.00	-12.5	4.6E-06
85	600.3	9.53	10.00	1.00	3.26	2.49	0.00	-5.00	-12.7	4.6E-06
86	700.1	9.68	10.00	1.00	3.41	3.06	0.00	0.00	-13.1	4.6E-06
87	700.1	9.62	10.00	1.00	3.41	3.06	-0.20	0.00	-13.2	4.6E-06
88	700.1	9.70	10.00	1.00	3.41	3.06	-0.20	-5.00	-12.4	4.6E-06
89	700.1	9.73	10.00	1.00	3.41	3.06	0.00	-5.00	-12.4	4.6E-06
90	800.4	9.89	10.00	1.00	3.82	3.30	0.00	0.00	-13.6	4.6E-06

Table 3 – Plasma potential, loss voltage (Vloss), and the full-width at half-maximum (FWHM) from the probe measurements two meters downstream of the NASA-173Mv2 at 10 mg/s.

	Plasma Potential (Volts from Ground)			
Vd	+IC, +OC	-ITC	-ITC, -ETC	-ETC
300	10.3	10.3	8.2	8.5
400	11.5	11.4	10.5	10.6
500	11.5	11.5	9.4	9.7
600	12.1	12	10.2	10.3
700	12.5	12.5	10.9	11
800	12.8	12.7	11.8	-
900	13.2	13.3	11.8	11.9
1000	13.5	13.5	12.3	12.2

	V_{loss} (Volts)			
Vd	+IC, +OC	-ITC	-ITC, -ETC	-ETC
300	34	34	34	35
400	34	-	-	32
500	32	33	33	34
600	32	28	28	28
700	26	27	25	24
800	25	-	-	-

	FWHM (Volts)			
Vd	+IC, +OC	-ITC	-ITC, -ETC	-ETC
300	35	38	33	33
400	47	-	-	48
500	55	55	53	49
600	75	75	73	71
700	96	92	91	93
800	105	-	-	-